

# Microscopic HFB+QRPA predictions of dipole strength for astrophysics applications

S. Goriely<sup>1</sup>, E. Khan<sup>2</sup>, M. Samyn<sup>1</sup>

<sup>1</sup>*Institut d'Astronomie et d'Astrophysique, ULB - CP226, 1050 Brussels, Belgium*

<sup>2</sup>*Institut de Physique Nucléaire, IN2P3-CNRS, 91406 Orsay, France*

---

## Abstract

Large-scale QRPA calculations of the E1 strength are performed on top of HFB calculations in order to derive the radiative neutron capture cross sections for the whole nuclear chart. The spreading width of the GDR is taken into account by analogy with the second-RPA (SRPA) method. The accuracy of HFB+QRPA model based on various Skyrme forces with different pairing prescription and parameterization is analyzed. It is shown that the present model allows to constrain the effective nucleon-nucleon interaction with the GDR data and to provide quantitative predictions of dipole strengths.

*Key words:* NUCLEAR REACTIONS: QRPA, E1-strength, Nuclear forces

*PACS:* 24.30.Cz,21.30.-x,21.60.Jz,24.60.Dr

---

## 1 Introduction

About half of the nuclei with  $A > 60$  observed in nature are formed by the so-called rapid neutron-capture process (or r-process) of nucleosynthesis, occurring in explosive stellar events. The r-process is believed to take place in environments characterized by high neutron densities ( $N_n \gtrsim 10^{20} \text{ cm}^{-3}$ ), so that successive neutron captures proceed into neutron-rich regions well off the  $\beta$ -stability valley forming exotic nuclei that cannot be produced and therefore studied in the laboratory. If the temperatures or the neutron densities characterizing the r-process are low enough to break the  $(n, \gamma) - (\gamma, n)$  equilibrium, the r-abundance distribution depends directly on the neutron capture rates by the so-produced exotic neutron-rich nuclei [1]. The neutron capture rates are commonly evaluated within the framework of the statistical model of Hauser-Feshbach (although the direct capture contribution can play an important role for such exotic nuclei). This model makes the fundamental assumption that the capture process takes place with the intermediary formation of a compound nucleus in thermodynamic equilibrium. In this approach, the Maxwellian-averaged  $(n, \gamma)$  rate at temperatures of relevance in r-process environments

strongly depends on the electromagnetic interaction, i.e the photon de-excitation probability. The well known challenge of understanding the r-process abundances thus requires that one be able to make reliable extrapolations of the E1-strength function out towards the neutron-drip line. To put the description of the r-process on safer grounds, a great effort must therefore be made to improve the reliability of the nuclear model. Generally speaking, the more microscopic the underlying theory, the greater will be one's confidence in the extrapolations out towards the neutron-drip line, provided, of course, the available experimental data are also well fitted.

Large scale prediction of E1-strength functions are usually performed using phenomenological Lorentzian models of the giant dipole resonance (GDR) [1]. Several refinements can be made, such as the energy dependence of the width and its temperature dependence [1–4] to describe all available experimental data. The Lorentzian GDR approach suffers, however, from shortcomings of various sorts. On the one hand, it is unable to predict the enhancement of the E1 strength at energies around the neutron separation energy demonstrated by various experiments, such as the nuclear resonance fluorescence. On the other hand, even if a Lorentzian-like function provides a suitable representation of the E1 strength for stable nuclei, the location of its maximum and its width remain to be predicted from some systematics or underlying model for each nucleus. For astrophysical applications, these properties have often been obtained from a droplet-type model [5]. This approach clearly lacks reliability when dealing with exotic nuclei, as already demonstrated by [6,7]. Recently an attempt was made to derive microscopically the E1 strength for the whole nuclear chart [7]. The dipole response was calculated with the Quasiparticle Random Phase Approximation (QRPA) on top of Hartree-Fock+BCS (HFBCS) description [8]. The only input of this approach was the Skyrme effective interaction injected in the HFBCS model. These microscopic calculations predicted the presence of a systematic low-lying component in the E1 strength for very neutron-rich nuclei. This low-lying component influences the neutron capture rate, especially if located in the vicinity of the neutron separation energy  $S_n$ .

In our previous HFBCS and QRPA microscopic approach [7], the pairing correlation in the BCS model was determined assuming a simple constant-gap pairing interaction. In addition, in the case of the highly neutron-rich nuclei that are of particular interest in the context of the r-process, the validity of the BCS approach to pairing is questionable, essentially because of the role played by the continuum of single-particle neutron states (see [9], and references therein). Therefore the impact of the newly-derived E1-strength functions on the cross section prediction could only be evaluated qualitatively. It was found that the radiative neutron capture cross sections by neutron-rich nuclei were systematically increased by the HFBCS+QRPA calculations [7] with respect to the one obtained using Lorentzian-like strength functions. Predictions with different forces have been compared, but no conclusions could be drawn regarding their intrinsic quality to predict the E1 strength. The final large-scale HFBCS+QRPA calculations performed in [7] were obtained on the basis of the Skyrme force denoted SLy4 [10].

In the present paper we calculate the dipole strength with one of the most accurate and reliable microscopic model available to date, namely the Hartree-Fock-Bogoliubov (HFB)

and QRPA models [11,12]. As recalled in Sect. 2.1, the ground state is described within the HFB model. Effective interactions of the Skyrme type characterized by different values of the nucleon effective mass and prescriptions for the pairing interaction are considered. The collective GDR mode is obtained by QRPA calculations on top of the HFB calculations, as described in Sect. 2.2. The residual interaction is derived self-consistently from the nucleon-nucleon effective interaction, which is the only input of the HFB calculation. To describe the damping of the collective motions on microscopic grounds, the second-RPA (SRPA) described by [13] is adopted (Sect. 2.3). This approach strongly improves the reliability of the predictions by eliminating the phenomenological spreading of the QRPA strength determined in our previous HFBCS+QRPA calculations [7]. This new approach allows us to determine on a more quantitative and reliable ground the photoabsorption cross section and consequently to judge the ability of the forces to reproduce experimental data. In order to select the most adequate interaction for the E1-strength calculation, the HFB+QRPA prediction are compared with photoabsorption data for 48 spherical nuclei [14,15] (Sect. 3). The HFB+QRPA predictions are further compared, in Sect. 3, with low-energy experimental data and generalized to include deformation effects in a phenomenological way. All these drastic improvements compared to the previous HFBCS and QRPA models allow to provide quantitative predictions of the E1-strength function, also for exotic neutron-rich nuclei (Sect. 4). The predicted GDR strengths are used to estimate all the radiative neutron capture rates of relevance for nucleosynthesis applications (Sect. 4).

## 2 HFB+QRPA calculation of the E1-strength function

The long-term goal of microscopic models is to describe on the same ground a wide variety of nuclear structure properties (in particular, magicity and pairing correlations in open-shell nuclei) for both stable and exotic nuclei. The HFB and QRPA models allows to treat, in a self-consistent way, pairing effects on the ground state as well as collective excitations for nuclei ranging from the valley of stability to the drip-line. The QRPA considers nuclear excitation as a collective superposition of two quasiparticle (qp) states built on top of the HFB ground state [16]. This collective aspect of the excitation makes the QRPA an accurate tool to investigate the E1-strength function, in both closed and open shell nuclei.

### 2.1 HFB Calculations

The HFB calculations considered in the present work are fully detailed in [17–20]. They are based on the conventional Skyrme force of the form

$$\begin{aligned}
v_{ij} = & t_0(1 + x_0 P_\sigma) \delta(\mathbf{r}_{ij}) + t_1(1 + x_1 P_\sigma) \frac{1}{2\hbar^2} \{p_{ij}^2 \delta(\mathbf{r}_{ij}) + h.c.\} \\
& + t_2(1 + x_2 P_\sigma) \frac{1}{\hbar^2} \mathbf{p}_{ij} \cdot \delta(\mathbf{r}_{ij}) \mathbf{p}_{ij} + \frac{1}{6} t_3(1 + x_3 P_\sigma) \rho^\gamma \delta(\mathbf{r}_{ij}) \\
& + \frac{i}{\hbar^2} W_0 (\boldsymbol{\sigma}_i + \boldsymbol{\sigma}_j) \cdot \mathbf{p}_{ij} \times \delta(\mathbf{r}_{ij}) \mathbf{p}_{ij} \quad .
\end{aligned} \tag{1}$$

The pairing force acting between like nucleons is treated in the full Bogoliubov framework with a  $\delta$ -function pairing force of the form [19–21]

$$v_\pi(\mathbf{r}_{ij}) = V_{\pi q} \left[ 1 - \eta \left( \frac{\rho}{\rho_0} \right)^\alpha \right] \delta(\mathbf{r}_{ij}) \quad , \tag{2}$$

where  $\rho$  is the density and  $\rho_0$  its equilibrium value in symmetric nuclear matter. Two types of pairing forces are considered here, a volume density-independent force characterized by  $\eta = 0$  and a volume plus surface (i.e density-dependent) force with  $\eta = 0.45$  and  $\alpha = 0.47$ . This latter prescription originates from the calculations of the pairing gap in infinite nuclear matter at different densities performed by Garrido et al. [21] using a “bare” or “realistic” nucleon-nucleon interaction. This density-dependent pairing has also been found to be compatible with experimental nuclear masses by [19], provided the space of single-particle states over which such a pairing force is allowed to act is truncated to about  $\varepsilon_\Lambda \simeq 15$  MeV around the Fermi energy. Note finally that in the present approach the strength parameter  $V_{\pi q}$  is allowed to be different for neutrons and protons, and also to be slightly stronger for an odd number of nucleons ( $V_{\pi q}^-$ ) than for an even number ( $V_{\pi q}^+$ ), i.e., the pairing force between neutrons, for example, depends on whether  $N$  is even or odd. For odd- $A$  and odd-odd nuclei, the blocking approximation is used, as detailed in [17].

Based on this Skyrme-HFB approach, a number of effective forces have been determined recently [18–20], the parameters of the underlying forces being fitted *exclusively* to all the 2135 available experimental masses [22], with some additional constraints regarding the stability of neutron matter and the incompressibility of nuclear matter. The parameters corresponding to these six forces named BSk2-BSk7 are summarized in Table 1. Are also included in Table 1 the effective isoscalar ( $M_s^*$ ), isovector ( $M_v^*$ ) nucleon mass and the root-mean-square (rms) deviations  $\sigma$  between the measured and estimated masses for the 2135 nuclei with  $Z, N \geq 8$ . More details about these forces can be found in [18–20]. The major differences between these six forces are found in the density-dependence of the pairing force and the adopted isoscalar effective nucleon mass. While BSk2 and BSk3 have been built without constraining the effective mass (leading to a value of  $M_s^*/M \gtrsim 1.04$ ), BSk4 and BSk5 are constrained by  $M_s^*/M = 0.92$ , as inferred from the extended Brückner-Hartree-Fock calculations of asymmetric nuclear matter [23] and BSk6 and BSk7 by  $M_s^*/M = 0.8$ , as inspired from the more traditional symmetric nuclear-matter calculations (e.g [24]). The mass-data fits with the BSk4–7 interaction are almost as good as those obtained with BSk2–3, in which  $M_s^*/M$  is unconstrained, so that such a mass fit cannot be used to discriminate between the different Skyrme forces and the corresponding optimal choice for the nucleon effective mass or the pairing interaction. For comparison purposes, we also consider the SLy4 Skyrme force [10] used in our previous HFBCS+QRPA calculation [7].

The SLy4 parameters are given in Table 1, the pairing interaction corresponding to the one determined in [12] (the mass rms deviation is however not available for the SLy4 force).

Table 1

Some properties of the Skyrme forces BSk2-BSk7 and SLy4 (see text for more details). The last line corresponds to the rms deviation between predicted and experimental masses for the full set of 2135 spherical and deformed nuclei.

	BSk2	BSk3	BSk4	BSk5	BSk6	BSk7	SLy4
$t_0$ [MeV fm <sup>3</sup> ]	-1790.63	-1755.13	-1776.94	-1778.89	-2043.32	-2044.25	-2488.91
$t_1$ [MeV fm <sup>5</sup> ]	260.996	233.262	306.884	312.727	382.127	385.973	486.818
$t_2$ [MeV fm <sup>5</sup> ]	-147.167	-135.284	-105.670	-102.883	-173.879	-131.525	-546.395
$t_3$ [MeV fm <sup>3+3γ</sup> ]	13215.1	13543.2	12302.1	12318.37	12511.7	12518.8	13777.0
$x_0$	0.4990	0.4766	0.5426	0.4445	0.7359	0.7292	0.834
$x_1$	-0.0898	-0.0326	-0.5352	-0.4887	-0.7992	-0.9323	-0.344
$x_2$	0.2244	0.4704	0.4947	0.5846	-0.3590	-0.0501	-1.0000
$x_3$	0.5157	0.4225	0.7590	0.5693	1.2348	1.2363	1.3540
$W_0$ [MeV fm <sup>5</sup> ]	119.05	116.07	129.50	130.70	142.38	146.93	123.00
$\gamma$	0.3433	0.3612	1/3	1/3	1/4	1/4	1/6
$V_{\pi n}^+$ [MeV fm <sup>3</sup> ]	-238	-359	-273	-429	-321	-505	-395
$V_{\pi n}^-$ [MeV fm <sup>3</sup> ]	-265	-407	-289	-463	-325	-514	-395
$V_{\pi p}^+$ [MeV fm <sup>3</sup> ]	-247	-365	-285	-447	-338	-531	-395
$V_{\pi p}^-$ [MeV fm <sup>3</sup> ]	-278	-413	-302	-483	-341	-541	-395
$\eta$	0	0.45	0	0.45	0	0.45	1.00
$\alpha$	0	0.47	0	0.47	0	0.47	1.50
$\varepsilon_\Lambda$ [MeV]	15	14	16	16	17	17	60
$M_s^*/M$	1.04	1.12	0.92	0.92	0.80	0.80	0.69
$M_v^*/M$	0.86	0.89	0.85	0.84	0.86	0.87	0.80
$\sigma$ [MeV]	0.674	0.656	0.680	0.675	0.686	0.676	–

## 2.2 QRPA Calculations

The E1-strength QRPA calculations are performed on top of the HFB results. The derivation of the QRPA response is detailed in [12], using Green's function formalism. The QRPA

response is obtained from the time-dependent HFB equations [16]:

$$i\hbar\frac{\partial\mathcal{R}}{\partial t} = [\mathcal{H}(t) + \mathcal{F}(t), \mathcal{R}(t)] \quad (3)$$

where  $\mathcal{R}$ ,  $\mathcal{H}$  are the time-dependent generalized density and HFB Hamiltonian respectively, and  $\mathcal{F}$  the external oscillating field. In the small amplitude limit the time-dependent HFB equations become:

$$\hbar\omega\mathcal{R}' = [\mathcal{H}', \mathcal{R}^0] + [\mathcal{H}^0, \mathcal{R}'] + [F, \mathcal{R}^0] \quad (4)$$

where ' stands for the perturbed quantity. The variation of the generalized density  $\mathcal{R}'$  is expressed in term of 3 quantities, namely  $\rho'$ ,  $\kappa'$  and  $\bar{\kappa}'$ , which are written as a column vector

$$\boldsymbol{\rho}' = \begin{pmatrix} \rho' \\ \kappa' \\ \bar{\kappa}' \end{pmatrix} . \quad (5)$$

Thus, at variance with the RPA, where one needs to know only the change of the particle-hole (ph) density ( $\rho'$ ), in QRPA one should calculate the variation of three basic quantities (Eq. 5). It should be noted that in the three dimensional space introduced above, the first dimension represents the ph subspace, the second the particle-particle (pp) one, and the third the hole-hole (hh) one. The response matrix has 9 coupled elements in QRPA, compared to one in the RPA formalism.

The variation of the HFB Hamiltonian is expressed in terms of the second derivatives of the HFB energy functional  $\mathcal{E}[\rho, \kappa, \bar{\kappa}]$  with respect to the densities

$$\mathcal{H}' = \mathbf{V}\boldsymbol{\rho}' , \quad (6)$$

where  $\mathbf{V}$  is the residual interaction matrix, namely :

$$\mathbf{V}^{\alpha\beta}(\mathbf{r}\sigma, \mathbf{r}'\sigma') = \frac{\partial^2\mathcal{E}}{\partial\rho_\beta(\mathbf{r}'\sigma')\partial\rho_\alpha(\mathbf{r}\sigma)}, \quad \alpha, \beta = 1, 2, 3. \quad (7)$$

Here, the notation  $\bar{\alpha}$  means that whenever  $\alpha$  is 2 or 3 then  $\bar{\alpha}$  is 3 or 2.

The quantity of interest is the QRPA Green's function  $\mathbf{G}$ , which relates the perturbing external field to the density change by

$$\boldsymbol{\rho}' = \mathbf{G}\mathbf{F} . \quad (8)$$

Replacing the above three equations in Eq. (4), yields the so-called Bethe-Salpeter equation

$$\mathbf{G} = (\mathbf{1} - \mathbf{G}_0\mathbf{V})^{-1} \mathbf{G}_0 = \mathbf{G}_0 + \mathbf{G}_0\mathbf{V}\mathbf{G} \quad (9)$$

corresponding to a set of 3x3 coupled equations. In Eq. (9), the unperturbed Green's

function  $\mathbf{G}_0$  is defined by :

$$\mathbf{G}_0^{\alpha\beta}(\mathbf{r}\sigma, \mathbf{r}'\sigma'; \omega) = \sum_{ij} \frac{\mathcal{U}_{ij}^{\alpha 1}(\mathbf{r}\sigma)\bar{\mathcal{U}}_{ij}^{*\beta 1}(\mathbf{r}'\sigma')}{\hbar\omega - (E_i + E_j) + i\eta} - \frac{\mathcal{U}_{ij}^{\alpha 2}(\mathbf{r}\sigma)\bar{\mathcal{U}}_{ij}^{*\beta 2}(\mathbf{r}'\sigma')}{\hbar\omega + (E_i + E_j) + i\eta} , \quad (10)$$

where  $E_i$  are the single qp energies and  $\mathcal{U}_{ij}$  are 3 by 2 matrices calculated from the  $U$  and  $V$  HFB wave functions [12].

In the case of transitions from the ground state to excited states within the same nucleus, only the (ph,ph) component of  $\mathbf{G}$  plays a role. If the interaction does not depend on spin variables the strength function is thus given by

$$S(\omega) = -\frac{1}{\pi} \text{Im} \int F^{11*}(\mathbf{r})\mathbf{G}^{11}(\mathbf{r}, \mathbf{r}'; \omega)F^{11}(\mathbf{r}')d\mathbf{r} d\mathbf{r}' . \quad (11)$$

The QRPA calculations are performed assuming the spherical symmetry. The residual interaction is derived from the interaction used in the HFB calculation (Eq. 7). The residual interaction corresponding to the velocity-dependent terms of the Skyrme force is approximated in the (ph,ph) subspace by its Landau-Migdal limit [25]. All the qp states are included up to an energy cutoff of 60 MeV, allowing pairs of qp energy up to 120 MeV. The strength distribution is calculated up to a maximum transition energy  $\omega_{max}=30$  MeV with a step of 100 keV and an averaging width  $\eta=150$  keV. In a fully consistent calculation the spurious center-of-mass state should come out at zero energy. Because of the Landau-Migdal form of the interaction adopted here, the consistency between mean field and residual qp interaction is broken and the isoscalar  $J^\pi = 1^-$  spurious state becomes imaginary. We cure this defect by renormalizing the residual interaction by a factor  $\alpha$  on the nuclei of interest. The spurious state comes out at zero energy with typical  $\alpha$  values between 0.85 and 1.

### 2.3 Second-RPA damping

The QRPA provides a reliable description of the GDR centroid and the fraction of the energy-weighted sum rule (EWSR) exhausted by the E1 mode. However, it is necessary to go beyond this approximation scheme in order to describe the damping properties of the collective motion. The GDR is known experimentally to have a large energy width and therefore a finite lifetime. Different microscopic theories exist (see e.g [13,26,27]).

In the previous HFBCS and QRPA calculation, the QRPA strength was folded by an arbitrary Lorentzian to generate the experimentally observed GDR width. We propose to describe the width on more microscopic grounds, by calculating it in the second-RPA (SRPA) framework [13]. The SRPA allows to take into account the spreading width due to the 2p-2h excitations. Formally, self-energy insertions on particle and hole lines spread the resonances and shift their centroids. In practice the ph QRPA strength is folded by a

Lorentzian function representing the self-energy operator [13,28]

$$f_L(E', E) = \frac{1}{2\pi} \frac{\Gamma(E)}{(E' - E - \Delta(E))^2 + \Gamma(E)^2/4} \quad . \quad (12)$$

where  $E'$  is the excitation energy of the ph-QRPA response,  $\Delta(E)$  and  $\Gamma(E)$  the real and complex part of the self-energy, respectively [13]. The energy dependent width  $\Gamma(E)$  can be calculated from the measured decay width of particle ( $\gamma_p$ ) and hole ( $\gamma_h$ ) states [13]

$$\Gamma(E) = \frac{1}{E} \int_0^E d\epsilon [\gamma_p(\epsilon) + \gamma_h(\epsilon - E)] (1 + C_{ST}) \quad . \quad (13)$$

The real part  $\Delta(E)$  of the self-energy is obtained from  $\Gamma(E)$  by a dispersion relation [13]. This empirical way of determining  $\Gamma(E)$  has the advantage of including, in principle, contributions from the excitation beyond 2p-2h [28]. The resulting resonance width can therefore be compared with experimental data, such as photoabsorption cross sections. The interference factor  $C_{ST}$  in Eq. (13) is due to the screening corrections of the exchange interaction which can interfere destructively with self-energy diagrams [13]. The microscopic evaluation of this factor is delicate. In practice,  $C_{ST}$  can be adjusted phenomenologically to reproduce experimental data [29], the same value being used for all nuclei. In our approach, it will be tuned to reproduce at best the 48 experimental GDR widths and peak energies in spherical nuclei [14,15], as shown in the next section.

### 3 Comparison with experimental data

#### 3.1 Photoabsorption data

Photo-induced reaction cross sections have been compiled by [14,15] and represent the most relevant and reliable source of experimental data with which HFB+QRPA predictions can be compared. These compilations provide the GDR parameters, i.e the peak energy, peak cross section and the full width at half maximum, observed in photonuclear reactions measured by bremsstrahlung, quasimonoenergetic and tagged photons for about 84 nuclei. Only photoabsorption data for the 48 spherical nuclei are considered at this stage, in order to free us from deformation effects. Figs. 1-3 compare the normalized experimental photoabsorption cross section with the QRPA predictions obtained with the 7 different Skyrme forces of Table 1. For each force, the interference factor  $C_{ST}$  is determined to reproduce at best the position of the peak energy and the full width at half maximum, simultaneously. As already stressed, the interference factor influences not only the GDR width, but also shifts the energy peak to higher energies. At energies around  $E \simeq 15$  MeV, the SRPA shifts the peak energy by approximately  $\Delta(E) \simeq 5 \times (1 + C_{ST})$  MeV upwards. For values  $C_{ST} \gtrsim -0.5$ , the GDR broadening becomes too large and incompatible with experimental photoabsorption data, while for values  $C_{ST} \lesssim -0.8$ , the fine structure inherent to the 1p-1h QRPA estimate is not smeared out enough by the SRPA and again incompatible with



experimental data. The final  $C_{ST}$  values are given in Table 2, as well as the rms deviations regarding the peak energy  $E_{GDR}$  and the full width at half maximum  $\Gamma_{GDR}$ .

Table 2

Interference factors adopted in the SRPA for the Skyrme forces BSk2-BSk7 and SLy4. Also given are the rms deviations for the peak energy  $E_{GDR}$  and the full width at half maximum  $\Gamma_{GDR}$  relative to the experimental values for the 48 spherical nuclei compiled in [14,15].

	BSk2	BSk3	BSk4	BSk5	BSk6	BSk7	SLy4
$C_{ST}$	-0.55	-0.55	-0.57	-0.55	-0.66	-0.63	-0.76
$\sigma(E_{GDR})$ [MeV]	1.217	1.664	0.702	0.630	0.541	0.445	0.847
$\sigma(\Gamma_{GDR})$ [MeV]	1.115	0.924	1.269	1.135	1.178	1.169	1.396

As illustrated in Figs. 1-3 and Table 2, the prediction of the GDR parameters is force-dependent. As far as the position of the peak energy is concerned, most of the forces overpredict the peak energy of light nuclei and underpredict it for the heavier species. The best agreement is found for the BSk6-7 forces which still overestimate  $E_{GDR}$  for the lightest elements, but give an excellent agreement for  $Z \gtrsim 40$  elements. It can be concluded that, within the present HFB+QRPA model, Skyrme forces need to have a low effective nucleon mass  $M_s^*/M \simeq 0.8$  to correctly predict the GDR characteristics. An effective mass as low as the one used in SLy4 requires a particularly low value of the interference factor (see Table 2) which simultaneously give rise to fine structure effects not observed experimentally (see Fig. 3).

Interestingly, the density dependence of the pairing interaction has a minor impact on the prediction of the E1-strength function. Almost no differences are found among the 2 couples of forces BSk4 vs BSk5 or BSk6 vs BSk7 (see in particular Fig. 3). Finally, note that the SRPA effect to shift the energy peak was not taken into account by the phenomenological Lorentzian damping adopted in our previous HFBCS+QRPA work [7], and obviously modifies the conclusion drawn regarding the ability of the SLy4 force to predict the location of the GDR. The agreement found here for the SLy4 interaction (Fig. 3) is worse than it used to be in [7] where an rms deviation of 0.457 MeV was obtained on the centroid energy for the same sample of spherical nuclei.

Finally, regarding the amplitude of the E1-strength function, the QRPA equations are solved so as to exhaust the Thomas-Reiche-Kuhn sum rule. This adopted EWSR corresponds to

$$\int_0^{\omega_{max}} \sigma(E) dE = 60 NZ/A \text{ [MeV b]} \quad (14)$$

and is found to reproduce well the peak cross section measured experimentally, as illustrated in Fig. 4. The resulting deviation can be characterized by an rms deviation factor  $f_{rms} = 1.18$  defined as

$$f_{rms} = \exp \left[ \frac{1}{N_e} \sum_{i=1}^{N_e} \ln^2 \frac{\sigma_{max}^i(th)}{\sigma_{max}^i(exp)} \right]^{1/2} \quad (15)$$

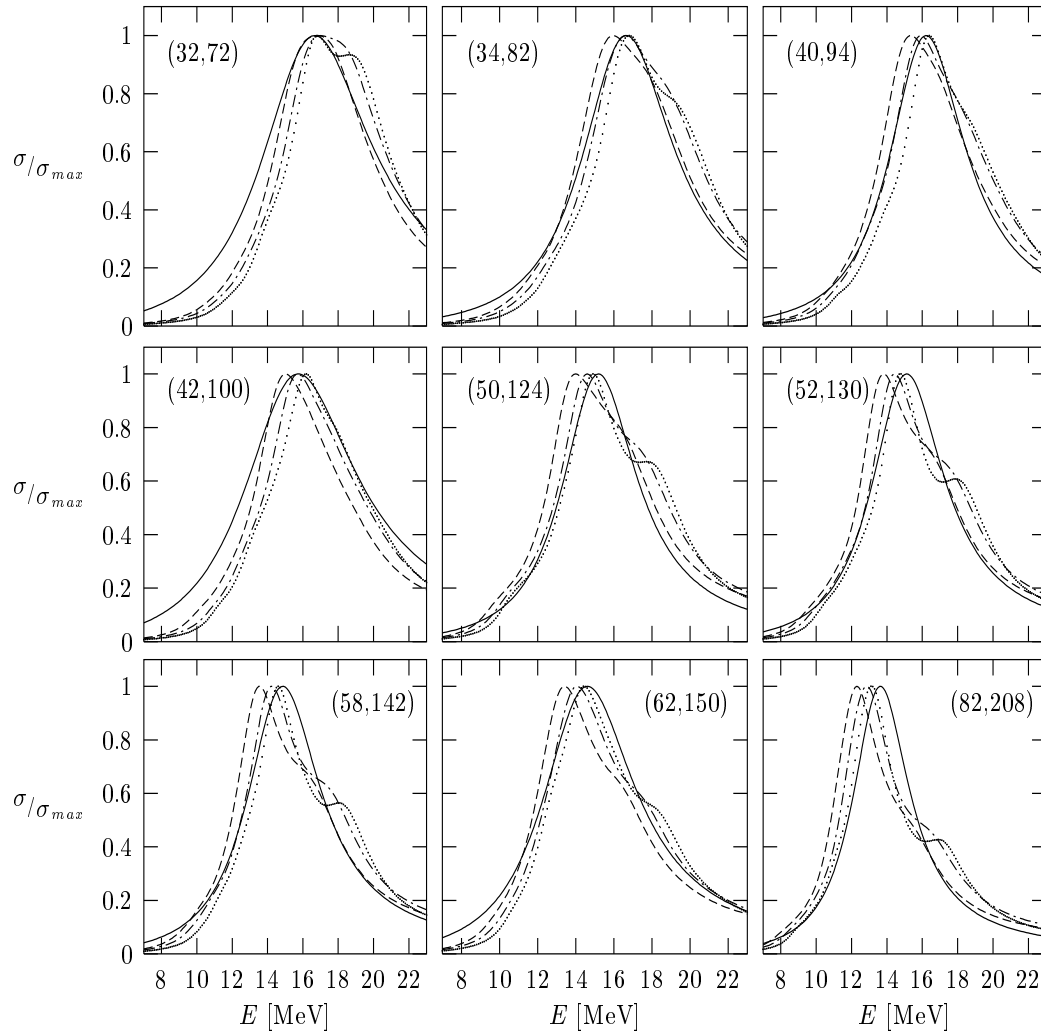


Fig. 1. Comparison between the experimental photoabsorption cross section approximated by a simple Lorentzian curve (solid line) in the vicinity of the peak energy [14] and the QRPA calculations obtained with the Skyrme forces BSk2 (dashed line), BSk4 (dash-dot line) and BSk6 (dotted line) for 9 representative spherical nuclei given by  $(Z, A)$ . All cross sections are normalized to a peak cross section of unity.

where  $\sigma_{max}(th)$  ( $\sigma_{max}(exp)$ ) is the theoretical (experimental) peak cross section and  $N_e = 48$  the number of nuclei in the experimental sample.

All these results show that among the six Skyrme forces studied here, both the BSk6 and BSk7 forces not only reproduce extremely well the experimental masses (with a rms deviation as low as 0.676 MeV on the 2135 known masses), but also is well adapted to describe the E1 collective excitations. For this reason, all further calculations are performed with BSk7 as our standard force. It should be stressed that for more than thirty years, phenomenological effective interactions were developed using exclusively ground state properties of nuclei, such as binding energies, radii or spectroscopic quantities. This was initiated through the Skyrme Hartree-Fock model by [30]. Nuclear forces are traditionally determined by fitting

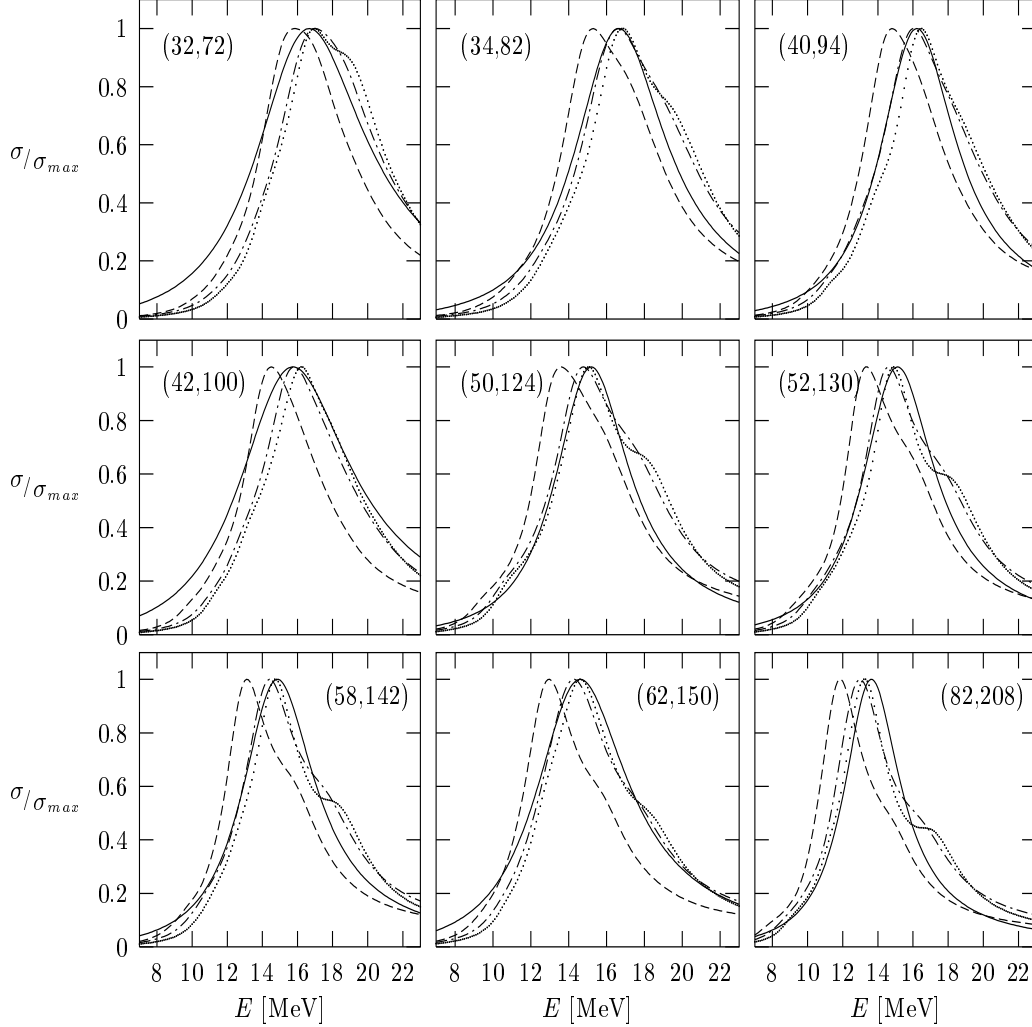


Fig. 2. Same as Fig. 1 with the Skyrme forces BSk3 (dashed line), BSk5 (dash-dot line) and BSk7 (dotted line).

such ground state properties for less than ten or so nuclei. Recently, progress has been achieved in determining the Skyrme force by fitting essentially all the mass data [17–20]. The only excited feature taken into account so far was the giant monopolar resonance energy [31] in order to predict the infinite matter compressibility modulus. The present HFB+QRPA model (with the SRPA corrections) allows to consider nuclear excitations such as GDR in the development of phenomenological effective interactions.

### 3.2 Generalization to deformed nuclei

In the case of deformed spheroidal nuclei, the GDR splits into two major resonances as a result of the different resonance conditions characterizing the oscillations of protons against neutrons along the axis of rotational symmetry and an arbitrary axis perpendicular to it.

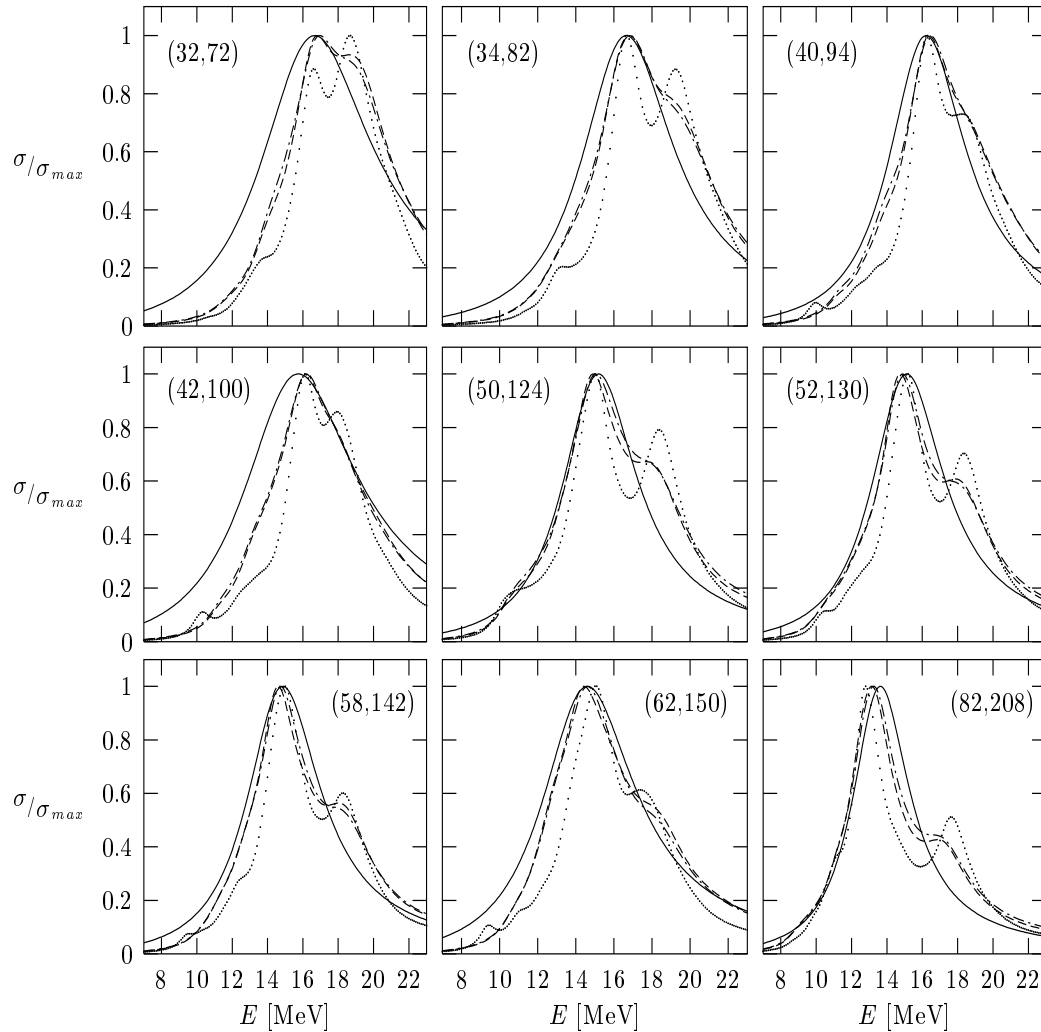


Fig. 3. Same as Fig. 1 with the Skyrme forces BSk6 (dashed line), BSk7 (dash-dot line) and SLy4 (dotted line).

In the phenomenological approach, the Lorentzian-type formula is generalized to a sum of two Lorentzian-type functions of energies  $E_{GDR}^l$  and width  $\Gamma_{GDR}^l$  [32], such that

$$\begin{aligned}
 E_{GDR}^1 + 2 E_{GDR}^2 &= 3E_{GDR} \\
 E_{GDR}^2/E_{GDR}^1 &= 0.911\eta + 0.089
 \end{aligned}
 \tag{16}$$

where  $\eta$  is the ratio of the diameter along the axis of symmetry to the diameter along an axis perpendicular to it. In turn, the width  $\Gamma_{GDR}^l$  of each peak is given by the same deformation dependence as the respective energy  $E_{GDR}^l$  [32]. A similar splitting of the resonance strength for deformed nuclei is applied within the SRPA procedure given by Eq. (12), the Lorentzian function at a given energy  $E'$  being split with an equal strength into two Lorentzian functions centered according to Eq. (16) and characterized by a width  $\Gamma(E)$  (see Eq. 13) obtained from the same relations (Eq. 16). As already found in [18], distributing

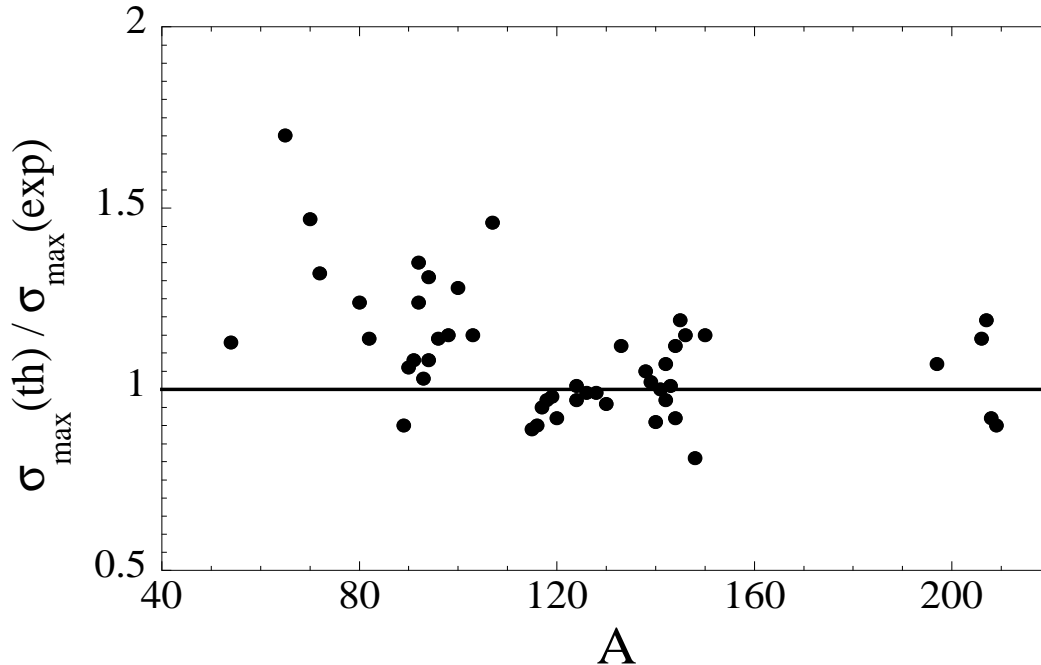


Fig. 4. Ratio of the peak cross section  $\sigma_{max}(th)$  estimated within the HFB+QRPA model with the BSk7 Skyrme force to the experimental value  $\sigma_{max}(exp)$  for the 48 spherical nuclei as a function of the mass number  $A$ .

the strength equally between the two resonance peaks gives optimal location and relative strength of both GDR centroid energies as observed experimentally. We illustrate in Fig. 5 how the photoabsorption cross section in  $^{235}\text{U}$  peaked around 12 MeV in the spherical approximation is split into the two observed peaks. The same deformation effects are applied to all nuclei predicted to be deformed by the HFB calculation based on the BSk7 force.

### 3.3 Low-energy E1-strength data

For practical astrophysics applications, it is of first importance to describe the tail of the GDR at low energies, i.e around the neutron separation energy, as reliably as possible [1]. Experimental E1 strengths at low energies are available through average resonance capture (ARC) data [33] or recent measurements of  $\gamma$ -ray spectra in light-ion reactions [34,35]. However, such data are related to the so-called “downwards” E1-strength function which determines the average width of the  $\gamma$ -decay, while the photoexcitation data considered so far depend on the “upwards” E1-strength function associated with  $\gamma$ -absorption. When dealing with  $\gamma$ -decay data, a temperature-dependent correction factor is traditionally introduced in the expression of the GDR width to take the collision of quasiparticles into account [3,33,36]. In order to guarantee the compatibility with photoabsorption data, we introduce in the SRPA procedure such a collision term by adding to the width  $\Gamma(E)$  (see

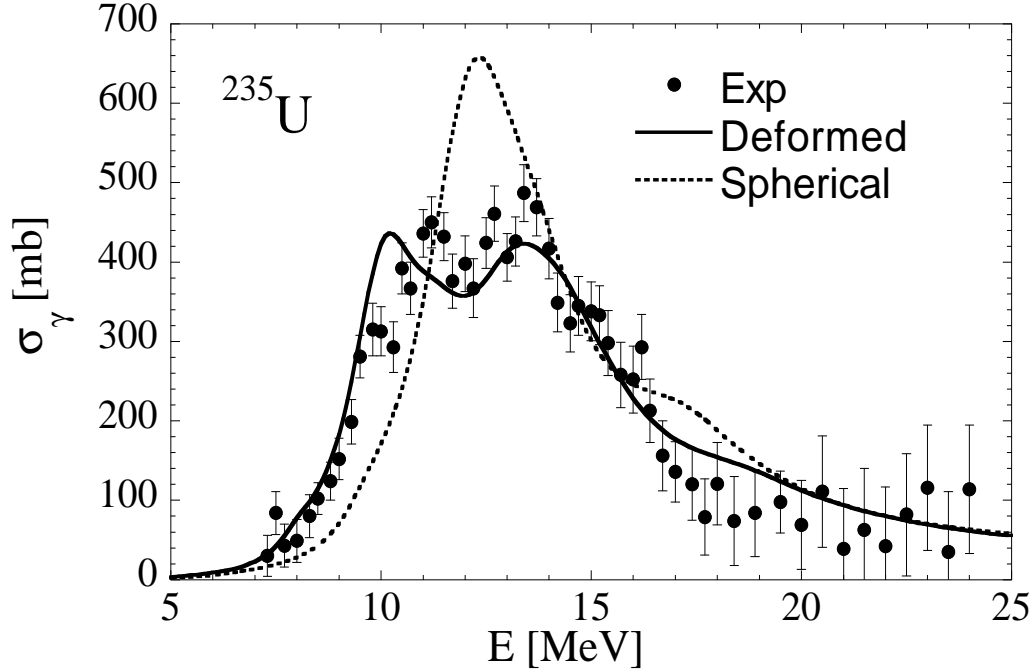


Fig. 5. Photoabsorption cross section for  $^{235}\text{U}$ . The dots correspond to experimental data [15]. The dotted line is the HFB+QRPA calculation obtained with the BSk7 force in the spherical approximation (applying the SRPA) and the full line when applying in addition our phenomenological procedure to describe deformation effects.

Eq. 13) a temperature-dependent correction term as

$$\Gamma'(E) = \Gamma(E) \left[ 1 + \alpha \frac{4\pi T^2}{E E_{GDR}} \right] \quad (17)$$

where  $T$  refers to the temperature of the absorbing state,  $E_{GDR}$  is the peak energy of the GDR and  $\alpha$  a normalization constant. In all calculations performed in the present work, the temperature is derived from the microscopic statistical model of nuclear level densities [37]. As shown below, adopting  $\alpha = 3$  gives excellent agreement with most of the available data.

Fig. 6 illustrates in the specific case of the spherical  $^{144}\text{Nd}$  nucleus, that the E1-strength data derived from primary photon spectra in the  $(n,\gamma)$  reaction around 6–8 MeV [33] or  $(n,\gamma\alpha)$  reaction around  $E \simeq 1$  MeV [38] are correctly reproduced at low energies with the  $T$ -dependent correction given by Eq. (17) with  $\alpha = 3$ . The energy dependence of the collision term introduced in Eq. (17) and already suggested in [1] is of particular importance, since it is responsible for the  $E \rightarrow 0$  behavior of the E1-strength function observed experimentally [33]. It is also found to affect the E1 strength around the neutron binding energy, as seen in Figs. 6–7.

In addition, we compare in Fig. 7 the QRPA predictions with the compilation of experimental E1-strength functions at low energies ranging from 4 to 8 MeV [39] for nuclei from  $^{25}\text{Mg}$  up to  $^{239}\text{U}$ . The data set includes resolved-resonance measurements, thermal-

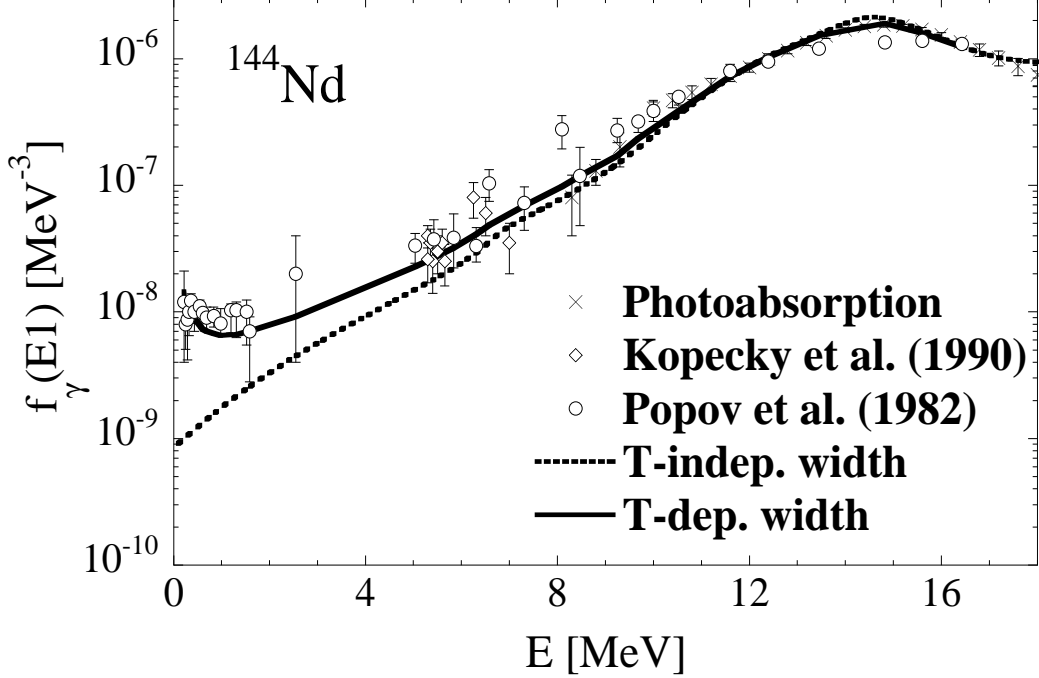


Fig. 6. Comparison of the photoabsorption data [14] and measured primary photon strength functions for  $(n, \gamma)$  reaction (crosses) [33] and  $(n, \gamma \alpha)$  reaction (circles) [38] with the QRPA predictions obtained with a  $T$ -independent (Eq. 13) and  $T$ -dependent (Eq. 17) width. The QRPA predictions are obtained with the BSk7 Skyrme force and a temperature  $T = 0.55$  MeV.

captures measurements and photonuclear data. In a certain number of cases the original experimental values need to be corrected, typically for non-statistical effects, so that only values recommended by [39] are considered in Fig. 7. QRPA predictions are globally in good agreement with experimental data at low energies in the whole nuclear chart. The average and rms deviations, as defined in Eq. (15), on the 62 experimental data have been estimated. The  $T$ -independent predictions underpredict the E1 strength by an average factor of 1.6, while on average the  $T$ -dependent formula (assuming  $\alpha = 3$  in Eq. 17) is in perfect agreement with the data. The respective rms deviation factors are  $f_{rms} = 2.6$  and 2.1 for the  $T$ -independent and  $T$ -dependent results. These results show that including a  $T$ -dependence in the E1 strength to describe the  $\gamma$ -decay data globally improves the agreement. A qualitative agreement is also obtained with the E1-strength function derived at low energy from primary photon spectra in light-ion reactions [34,35], although the fine structure pattern are not reproduced.

#### 4 Extrapolation to neutron-rich nuclei and application to the radiative neutron capture

Large-scale QRPA calculations based on the BSk7 Skyrme force have been performed for all  $8 \leq Z \leq 110$  nuclei lying between the proton and the neutron driplines, i.e some 8300 nuclei. The SRPA is applied to all distributions. In the neutron-deficient region, as well

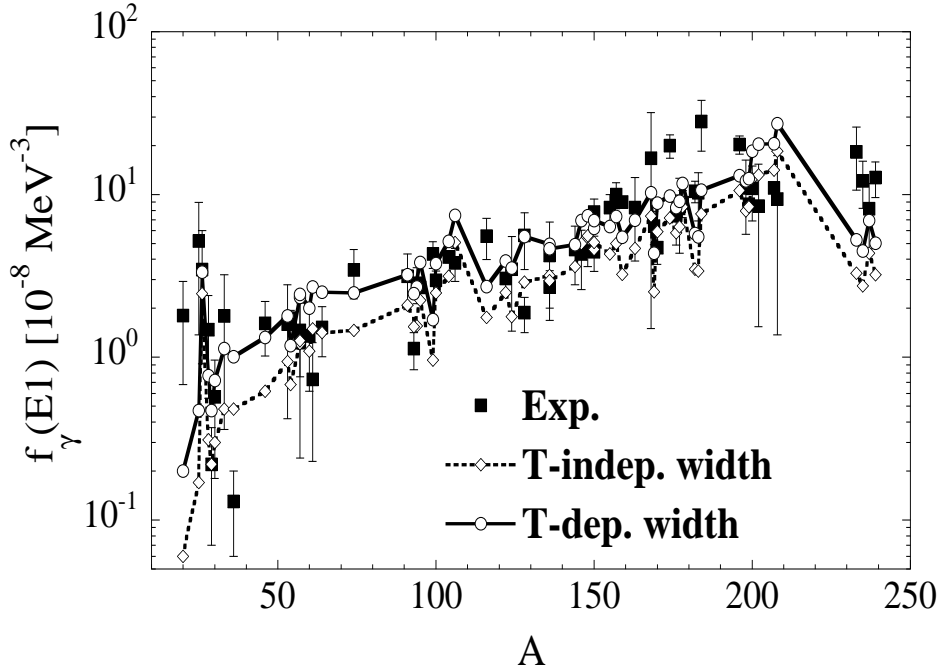


Fig. 7. Comparison of the QRPA  $T$ -dependent and  $T$ -independent low-energy E1-strength functions with the experimental compilation [39] including resolved-resonance and thermal-captures measurements, as well as photonuclear data for nuclei from  $^{25}\text{Mg}$  up to  $^{239}\text{U}$  at energies ranging from 4 to 8 MeV.

as along the valley of  $\beta$ -stability, the resulting E1-strength functions are very similar to the empirical Lorentzian-like approximation. When dealing with neutron-rich nuclei, the QRPA predictions start deviating from a simple Lorentzian shape and results quantitatively similar to [7] are obtained. In particular, some extra strength is found to be located at an energy lower than the GDR energy. The more exotic the nucleus, the stronger this low-energy component. This is illustrated in Fig. 8 for the E1-strength function in the Sn isotopic chain. All nuclei shown in Fig. 8 are predicted to be spherical in the HFB calculations based on the BSk7 force [20]. For the  $A \geq 140$  neutron-rich isotopes, an important part of the strength is concentrated at low energies ( $E \lesssim 5 - 7$  MeV). Phenomenological models are unable to predict such low energy components. In particular for  $^{150}\text{Sn}$ , all phenomenological systematics (as used for cross section calculation) predict a  $\gamma$ -ray strength peaked around 15 MeV with a full width at half maximum of about 4.5 MeV [39] which is obviously very different from the microscopic estimate (Fig. 8). More generally, the present HFB+QRPA calculation confirms that the neutron excess affects the spreading of the isovector dipole strength, as well as the centroid of the strength function. The energy shift is larger than predicted by the usual  $A^{-1/6}$  or  $A^{-1/3}$  dependence given by the phenomenological liquid drop approximations [5]. The above-described feature of the QRPA E1-strength function for nuclei with a large neutron excess is qualitatively independent of the adopted effective interaction.

The radiative neutron capture cross section is estimated within the statistical model of Hauser-Feshbach making use of the MOST code [40]. It should be noted that this ver-



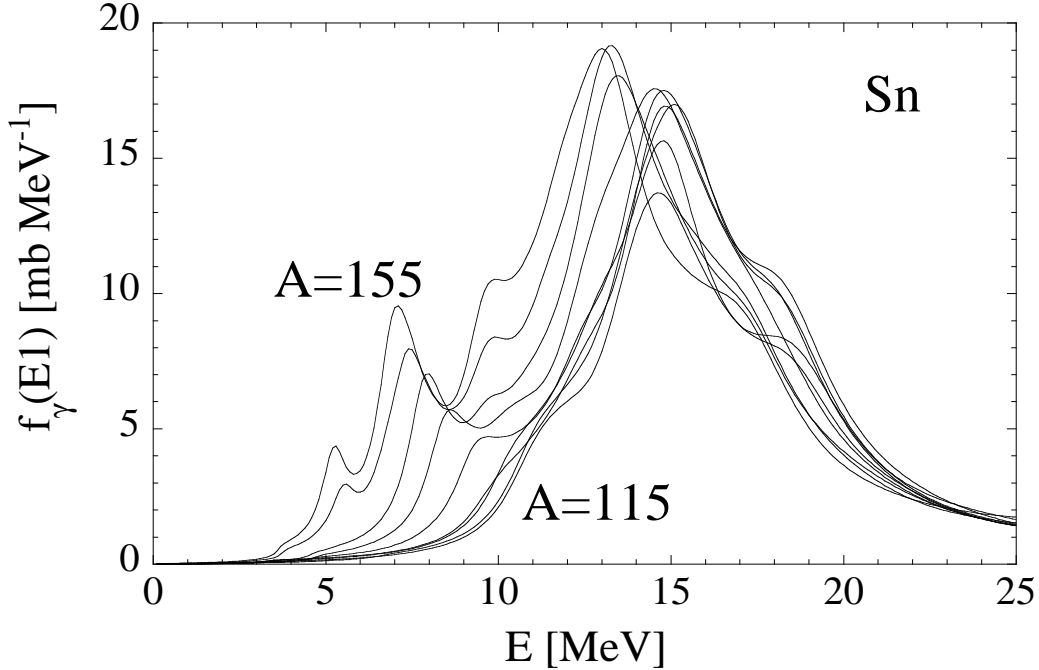


Fig. 8. E1-strength function for the Sn isotopic chain predicted by the HFB+QRPA with the BSk7 force. The SRPA is applied to all distribution. Only isotopes ranging between  $A=115$  and  $A=150$  by steps of  $\Delta A=5$  are displayed.

sion makes use of the nuclear ground state properties derived coherently from the same microscopic HFB method with the BSk7 Skyrme force [20]. It also benefits from the improved nuclear level density prescription based on the microscopic statistical model, also used to estimate the nuclear temperature in Eq. (17) [37]. The direct capture contribution as well as the possible overestimate of the statistical predictions for resonance-deficient nuclei are effects that could have an important impact on the radiative neutron captures by exotic nuclei [1], but are not included in the present study. The Maxwellian-averaged radiative neutron capture rate at a temperature  $T = 1.5 \cdot 10^9$  K, typical of the r-process nucleosynthesis, obtained with the QRPA E1-strength are compared in Fig. 9 with those based on the Hybrid Lorentzian-type formula [1]. These rates are sensitive to the neutron capture cross section at incident energies around 130 keV, and therefore depend on the E1 strength in a narrow range of a few hundred keV around  $S_n$ . The temperature-dependent Hybrid formula corresponds to a generalization of the energy- and temperature-dependent Lorentzian formula including an improved description of the E1-strength function at energies below  $S_n$  as derived from [3]. The Hybrid E1 strength differs from the QRPA estimate not only in the location of the centroid energy, but also in the low-energy tail. No extra low-lying strength is included in the phenomenological Hybrid formula, but its temperature dependence increases the E1 strength at low energies and is responsible for its non-zero  $E \rightarrow 0$  limit. The newly-derived strength gives an increase of the rate by a factor up to 6 close to the neutron drip line. R-process nuclei characterized by  $S_n \lesssim 3$  MeV are seen to have a neutron capture rate about at least twice faster than the one predicted with the phenomenological Hybrid formula. This is due to the shift of the GDR to lower energies compared with the usually adopted liquid-drop  $A^{-1/3}$  rule, as well as to the appearance of

some extra strength at low energies as explained above. Both effects tend to increase the E1 strength at energies below the GDR, i.e in the energy window of relevance in the neutron capture process. For less exotic nuclei, the QRPA impact is relatively small, differences being mainly due to the exact position of the GDR energy and the resulting low-energy tail. When compared to our previous HFBCS+QRPA predictions [7], the HFB+QRPA model gives larger neutron capture rates close to the neutron drip line, but lower rates for many of the  $4 \lesssim S_n$  [MeV]  $\lesssim 2$  nuclei, as seen in Fig. 9 (lower panel). These differences justify the use of the HFB approach for exotic neutron-rich nuclei.

## 5 Conclusions

The E1-strength function is estimated with one of the most accurate and reliable microscopic model available to date, namely the Hartree-Fock-Bogoliubov (HFB) and QRPA models. The spreading width of the GDR is taken into account by analogy with the SRPA method. The analysis of HFB+QRPA model based on various Skyrme forces with different pairing prescriptions and parameterizations shows that the effective nucleon-nucleon interaction can be constrained with the GDR data. In particular, it is found that the Skyrme force characterized with a low effective mass  $M_s^*/M \simeq 0.8$  is a necessary condition to reproduce the location and width of the GDR, at least within the present HFB+QRPA model to which the SRPA is applied. In contrast, GDR data cannot be used to discriminate between the surface or volume property of the pairing interaction. In addition to its reliability, it is shown that the HFB+QRPA model also gives accurate predictions and that globally it agrees fairly well with experimental data. The present HFB+QRPA model brings important improvement with respect to our previous HFBCS+QRPA model and can provide quantitative predictions of the dipole strength. Large-scale calculations of the E1-strength function are performed and used to estimate the radiative neutron capture rates of relevance for the r-process nucleosynthesis. A systematic increase of the reaction rates for exotic neutron-rich nuclei is found.

Further improvements may be useful. A proper treatment of the continuum states and its impact on the dipole strength is an important issue. It is expected to be significant for drip-line nuclei. Continuum-QRPA models are available [12] and study along these lines are in progress. The particle-vibration coupling also affects the low-energy strength and could contribute to an extra increase of the radiative neutron capture rate by exotic nuclei.

**Acknowledgments** M.S. and S.G. are FNRS Research Fellow and Associate, respectively. This work has been performed within the scientific collaboration (Tournesol) between the Wallonie–Bruxelles Community and France.

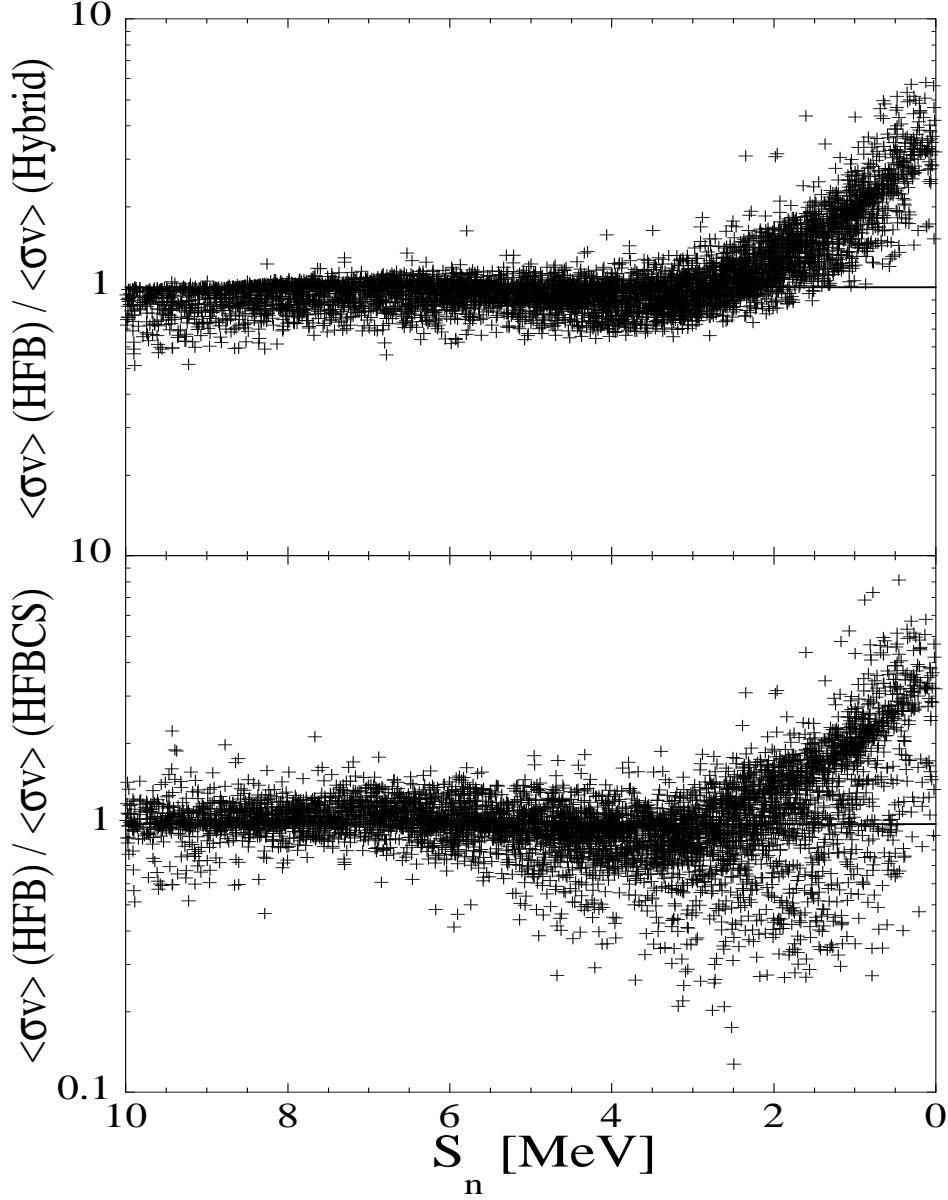


Fig. 9. Upper panel: Ratio of the Maxwellian-averaged  $(n, \gamma)$  rate (at a temperature of  $1.5 \cdot 10^9$  K) obtained with the HFB+QRPA E1 strength to the one using the Hybrid formula [1] as a function of the neutron separation energy  $S_n$  for all nuclei with  $8 \leq Z \leq 110$ . Lower panel: Same as upper panel where the HFB+QRPA neutron capture rates are compared with the HFBCS+QRPA rates of [7].

## References

- [1] S. Goriely, Phys. Lett. B436 (1998) 10.
- [2] C.M. McCullagh, M.L. Stelts, R.E. Chrien, Phys. Rev. C23 (1981) 1394.
- [3] S.G. Kadenskii, V.P. Markushev, V.I. Furman, Sov. J. Nucl. Phys. 37 (1983) 165.

- [4] J. Kopecky, R. E. Chrien, Nucl. Phys. A468 (1987) 285.
- [5] W.D. Myers, W.J. Swiatecki, et al., Phys. Rev. C15 (1977) 2032.
- [6] F. Catara, E.G. Lanza, M.A. Nagarajan, A. Vitturi, Nucl. Phys. A624 (1997), 449.
- [7] S. Goriely, E. Khan, Nucl. Phys. A706 (2002) 10.
- [8] E. Khan, Nguyen Van Giai, Phys. Lett. B472 (2000) 253.
- [9] J. Dobaczewski, W. Nazarewicz, T.R. Werner, J.F. Berger, C.R. Chinn, J. Decharge, Phys. Rev. C53 (1996) 2809.
- [10] E. Chabanat, P. Bonche, P. Haensel, J. Meyer, R. Schaeffer, Nucl. Phys. A635 (1998) 231.
- [11] M. Grasso, N. Sandulescu, Nguyen Van Giai, R. J. Liotta, Phys. Rev. C64 (2001) 064321.
- [12] E. Khan, N. Sandulescu, Nguyen Van Giai, M. Grasso, Phys. Rev. C66 (2002) 024309.
- [13] S. Drożdż, S. Nishizaki, J. Speth, J. Wambach, Phys. Rep. 197 (1990) 1.
- [14] S.S. Dietrich, B. L. Berman, At. Data Nucl. Data Tables 38 (1989) 199.
- [15] Photonuclear data for applications; cross sections and spectra, IAEA-Tecdoc-1178 (2000).
- [16] P. Ring, P. Schuck, *The nuclear many-body problem*, Springer-Verlag (1980).
- [17] M. Samyn, S. Goriely, P.-H. Heenen, J.M. Pearson, F. Tondeur, Nucl. Phys. A700 (2002) 142.
- [18] S. Goriely, M. Samyn, P.-H. Heenen, J.M. Pearson, F. Tondeur, Phys. Rev. C 66 (2002) 024326.
- [19] M. Samyn, S. Goriely, J.M. Pearson, Nucl. Phys. A (2003) submitted.
- [20] S. Goriely, M. Samyn, M. Bender, J.M. Pearson, Nucl. Phys. A (2003) in preparation.
- [21] E. Garrido, P. Sarriguren, E. Moya de Guerra, P. Schuck, Phys. Rev. C 60 (1999) 064312.
- [22] G. Audi, A.H. Wapstra, private communication (2001).
- [23] W. Zuo, I. Bombaci, U. Lombardo, Phys. Rev. C **60**, 024605 (1999).
- [24] J.P. Jeukenne, A. Lejeune, C. Mahaux, Phys. Rep. **25**, 83 (1976).
- [25] S.O. Bäckman, A.D. Jackson, J. Speth, Phys. Lett. B56 (1975) 209.
- [26] G. Colò, P.F. Bortignon, Nucl. Phys. A696 (2001) 427.
- [27] P. Schuck, S. Ayik, Nucl. Phys. A687 (2001) 220c.
- [28] R.D. Smith, J. Wambach, Phys. Rev. C38 (1988) 100.
- [29] F.T. Baker, L. Bimbot, C. Djalali, et al., Phys. Rep. 289 (1997) 235.
- [30] D. Vautherin, J.D.M. Brink, Phys. Rev. C5 (1972) 626.
- [31] Nguyen Van Giai, H. Sagawa, Nucl. Phys. A371 (1981) 1.

- [32] F.-K. Thielemann, M. Arnould, in: Proceedings of Conference on Nuclear Data for Science and Technology, (eds. K. Böckhoff, Reidel, Dordrecht, 1983) 762.
- [33] J. Kopecky, M. Uhl, Phys. Rev. C41 (1990) 1941.
- [34] A. Voinov, M. Guttormsen, E. Melby, J. Rekstad, A. Schiller, S. Siem, Phys. Rev. C **63**, 044313 (2001).
- [35] S. Siem, M. Guttormsen, K. Ingeberg, E. Melby, J. Rekstad, A. Schiller, A. Voinov, Phys. Rev. C **65**, 044318 (2002).
- [36] P.F. Bortignon, Nucl. Phys. A687 (2001) 329c.
- [37] P. Demetriou, S. Goriely, Nucl. Phys. A695 (2001) 95.
- [38] Yu.P. Popov, In Proc. Europhys. Top. Conf., Physics and Application, Vol. 10 (Ed. P. Oblozinsky), p. 121 (1982).
- [39] Reference Input Parameter Library, IAEA-Tecdoc, in press (2003).
- [40] S. Goriely, 2001, in Tours Symposium on Nuclear Physics III, AIP Conf. Proc. 561, eds. M. Arnould et al. (New York: AIP), 53; <http://www-astro.ulb.ac.be>.